Electronic stabilization of a 5×4 dopant superlattice on Si(111)5×2-Au

J. L. McChesney,[1] J. N. Crain,[1] V. Pérez-Dieste,[1] Fan Zheng,[1] M. C. Gallagher,[2] M. Bissen,[3] C. Gundelach,[3] and F. J. Himpsel[1]

[1]*Department of Physics, UW-Madison, 1150 University Avenue, Madison, Wisconsin 53706, USA*

[2]*Department of Physics, Lakehead University, Thunder Bay, ON Canada, P7B-5E1*

[3]*Synchrotron Radiation Center, UW-Madison, 3731 Schneider Drive, Stoughton, Wisconsin 53589, USA*

(Received 2 March 2004; revised manuscript received 21 July 2004; published 23 November 2004)

The Si(111)5×2-Au surface exhibits a chain structure with additional Si atoms on top of the chains. They dope the chains to achieve the optimum band filling, according to recent local density calculations. Surprisingly, the Si atoms form a half-filled, disordered 5×4 lattice fluid, not an ordered 5×8 lattice. From their autocorrelation function an interatomic potential with 5×4 periodicity was deduced. An explanation for the 5×4 periodicity is provided by establishing a connection to the electronic structure near the Fermi level E_F, which is mapped by angle-resolved photoemission. The constant energy surfaces near E_F consist of one-dimensional lines at the boundaries of a 5×4 Brillouin zone. Such nested features of high density of states are capable of triggering a 5×4 superlattice interaction. The measurements establish a two-way connection between electronic structure and interatomic potentials: A one-dimensional Fermi surface instability triggers a superlattice of extra atoms, and the atoms provide the correct number of electrons for such an instability to occur. The band structure is discussed in view of the recently observed phase-separation into nanometer-sized segments of metallic and semiconducting character.

DOI: 10.1103/PhysRevB.70.195430 PACS number(s): 73.20.At, 79.60.Jv, 73.22.Dj, 73.21.Hb

I. INTRODUCTION

The electronic and structural properties of one-dimensional solids are predicted to be fundamentally different from those in higher dimensions.[1–3] Single particle excitations are replaced by collective excitations, since the wave functions of electrons moving along a line are forced to overlap strongly and thus to become highly correlated. Examples are charge and spin density waves and pairing in superconductors. Long-range order collapses in one dimension unless there are long-range interaction potentials stabilizing it. As a consequence, one-dimensional structures are prone to a variety of structural and electronic instabilities.[3] The Peierls distortion, for example, combines a doubling of the unit cell with a metal-insulator transition.

In the following, we explore the origin of structural instabilities occurring in one-dimensional chain structures at silicon surfaces,[4] triggered by extra atoms on top of the chains. The Si(111)5×2-Au surface is used as a prototype for a whole class of similar chain structures that are induced by metals on vicinal Si(111). The additional atoms interact with the underlying chains by doping them, and the chains in return provide a periodic holding potential for the adatoms. For various chain structures we have observed superlattices with a doubled, tripled, and quadrupled period. The Si(111)5×2 surface forms a 5×4 superlattice, but only half of the lattice sites are occupied by extra Si atoms. The origin of this superlattice is still unclear. It is the goal of this work to find a possible connection to the electronic structure of the chains, thus connecting a structural with an electronic instability. Extrapolating the Peierls model one might expect that atom-atom interactions are driven by the energetics established by the electrons near the Fermi level, but such a connection has been difficult to establish experimentally.

Silicon is a convenient substrate for the formation of one-dimensional chain structures for several reasons. The band gap of silicon prevents metallic chain states near the Fermi surface from coupling to the substrate. Already the flat Si(111) surface breaks its threefold symmetry with a submonolayer coverage of metal atoms and forms three domains of anisotropic $n\times1$ structures for many metals.[4] With gold atoms it is possible to achieve metallic chain structures at many vicinal Si(111) surfaces.[5–26] They can drive atomic rearrangements via instabilities of the high energy electrons at the Fermi surface, such as a Peierls distortion.[20]

Here we focus on the Si(111)5×2-Au structure, which is one of the best-known chain structures on Si.[5–16] First principles calculations of the electronic structure are becoming available[24,25] and a structural model has been proposed based on total energy minimization.[25] The latter is not only consistent with the chain structure seen by scanning tunneling microscopy (STM) but also with the strongest electron energy band observed in angle-resolved photoemission. Even finer details, such as a gradual transition from one-dimensional behavior near the top of this band to two-dimensional near the bottom[10] are accounted for in this model.[25] While the strongest band is well established, its contribution to structural instabilities of the surface atoms is probably small, because the band maximum lies well below the Fermi level E_F (at −0.3 eV). Weaker bands exist closer to E_F, but their characteristics have not been pinpointed. It is not even clear whether they make the surface metallic[6,8,9,13] or semiconducting.[15] Recent scanning tunneling spectroscopy results[16] offer a resolution of this puzzle by observing that the chain structure converts from metallic to semiconducting when extra Si atoms are located on top of the chain in a 5×4 superlattice. Thus, one may have to explain the observed band structure in terms of two sets of bands, one for sections

without Si adatoms, the other for sections with a 5×4 adatom lattice.

The tendency of the Si(111)5×2-Au surface to separate into these two phases is also visible in STM studies that investigate the use of this surface as storage medium for an atomic scale memory.[27–29] The limit of the storage density is determined by residual correlations between the Si adatoms that store the bits. From those correlations the potential acting between the Si adatoms can be obtained.[29] It contains a 1.2 meV term with 5×4 periodicity that is connected with the tendency to form short 5×4 adatom chains. In order to obtain the equilibrium coverage of 50% for the 5×4 lattice, there have to be empty segments between the 5×4 adatom chains. Without such a phase separation one would need a 5×8 lattice to accommodate the equilibrium coverage, but that is not observed. A fully occupied 5×4 structure can actually be prepared by depositing the missing $1/40$ of a monolayer of Si atoms, but it is only metastable and reverts to 50% filling at temperatures above 300 °C.[28]

In the following we will use detailed maps of the energy bands near the Fermi level to reveal two bands that are relevant to the energetics of the surface reconstruction. Both come closest to E_F at the boundaries of a 5×4 Brillouin zone, which makes them prime candidates for triggering a 5×4 superlattice by forming minigaps at E_F. One of them is semiconducting with a gap of $\geqslant$0.04 eV below E_F. The other is metallic within the limits of the absolute energy calibration. It exhibits a fairly high Fermi velocity of 0.74×10^6 m/s. Possible assignments of the observed bands in view of the recently reported two-phase model are discussed, where sections with 5×4 adatom chains were found to be semiconducting and adatom-free sections metallic.[16]

II. EXPERIMENT

The deposition of gold on Si(111)7×7 at temperatures above 600 °C leads to the 5×2 chain reconstruction, which breaks the threefold symmetry of Si(111).[5–16] After preparing the stepped Si(111) template[30] we deposit the precise gold coverage[5] of 0.4 ML [in units of Si(111) surface layers], which corresponds to two Au chains per unit cell. After Au deposition at 650 °C the surface is annealed to 850 °C for a few seconds, followed by slow cooling over several minutes. The details of the annealing sequence have been reported previously.[10,12,30]

For flat Si(111) substrates the length of the chains is limited by the domain structure of the three equivalent chain directions $[1\bar{1}0]$, $[01\bar{1}]$, $[\bar{1}01]$. Slightly stepped silicon surfaces break the threefold symmetry of the substrate and favor a single domain if the step edge is chosen along one of the three equivalent chain directions. We use a tilt of the surface normal by 1° towards the $[\bar{1}\bar{1}2]$ azimuth. On these substrates we are able to prepare very pure single-domain Si(111)5×2-Au surfaces, as long as the crystal is kept stress-free during heating and the heating current runs parallel to the steps. Figure 1 shows a low-energy electron diffraction (LEED) pattern of such a structure, where not even a trace of a second domain can be made out. This is particularly important for mapping the electronic states near the Fermi surface, which exhibit large intensity variations through different Brillouin zones. A strongly emitting band from a weak second domain can easily produce a photoemission intensity comparable to that of a weak band from the primary domain.

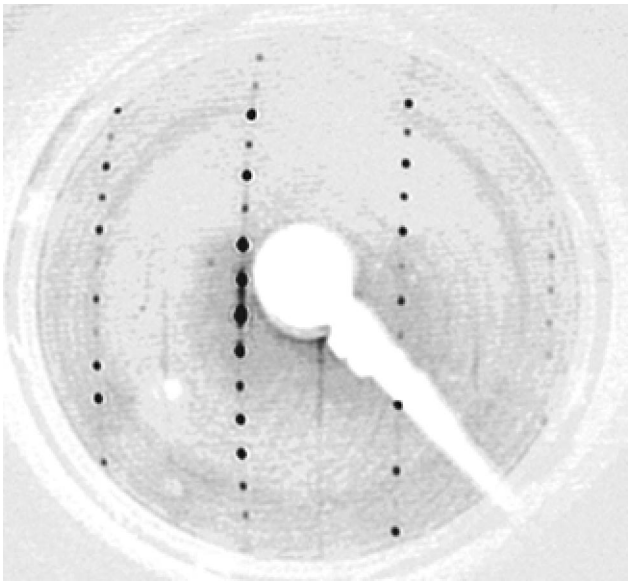

FIG. 1. LEED pattern of a single domain Si(111)5×2-Au surface, obtained from a vicinal surface tilted by 1° towards the $[\bar{1}\bar{1}2]$ azimuth at 87 eV. Between the rows of $1/5$-order spots there are weak $1/2$-order streaks that indicate long 5×2 domains along the chains but little correlation perpendicular to the chains.

Band dispersions and Fermi surfaces were obtained using a Scienta 200 spectrometer with E,ϑ multidetection and an energy resolution of 20 meV for electrons and 7 meV for photons (see Ref. 31 about details on the acquisition of Fermi surfaces). We used *p*-polarized synchrotron radiation at a photon energy $h\nu=34$ eV, where the cross section of silicon surface states has a maximum relative to the bulk states.[12,32] Figure 2 displays the band dispersion $E(k_x)$ along the chain direction. The photoemission intensity is plotted in a gray scale with high intensity shown dark. A shallow high-pass filter eliminates slow intensity variations and makes the $E(k_x)$ relation better visible. The Fermi surface is plotted in Fig. 3 together with a deeper energy surface near the top of the strongest band. The data are for a sample temperature of $<$100 K. The band dispersions in Fig. 1 are given with respect to the Fermi level E_F. The position of the valence band maximum (VBM) of Si ranges from 0.1 to 0.3 eV below E_F according to several previous measurements.[7,14,15] At low temperatures we find a substantial photovoltage (−0.93 eV for *n*-type and +0.06 eV for *p*-type samples). Since the absolute value of the photovoltage is a lower bound for the Schottky barrier (E_F—VBM for *p*-type, conduction band minimum—E_F for *n*-type) we obtain the constraint $0.06\text{ eV}<E_F\text{—VBM}<0.22$ eV. In order to keep the sample potential well defined we saturated the photovoltage by illumination with an extra spotlight. Thereby, residual variations in the sample potential with angle were kept to about 0.08 eV, which is taken as overall uncertainty of the band energies.

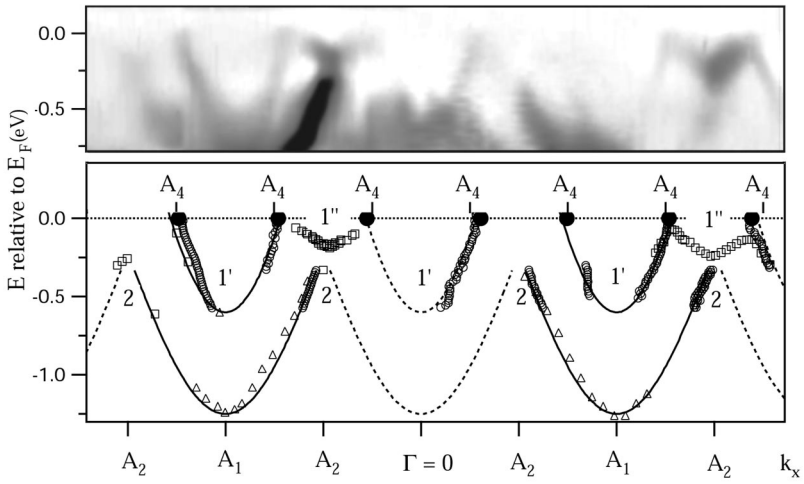

FIG. 2. Band dispersions of Si(111)5×2-Au along the chain direction k_x (with $k_y=0$). The photoemission intensity is represented as gray scale image (high intensity shown dark). The data can be modeled by three bands **1′**,**1″** and **2**. Bands **1′**,**1″** approach the Fermi level E_F at the boundaries A_4 of the 5×4 Brillouin zone. The top of band **2** lies 0.3 eV below E_F at the boundary A_2 of the 5×2 zone. The A_2 points lie at $k_x = \pm 0.41, \pm 1.23$ Å^{-1}.

III. BAND DISPERSIONS AND FERMI SURFACE

A quick glance at the constant energy surfaces in Fig. 3 reveals that the band structure is highly one-dimensional near the Fermi level. The energy surfaces consist of straight lines perpendicular to the chains (along k_y), as expected for a one-dimensional structure. There is a significant intensity modulation due to dipole selection rules, but very little curvature from two-dimensional coupling (compare other chain structures where residual two-dimensional coupling introduces an undulation of the Fermi lines[21,22]). Farther down in energy the band dispersion becomes gradually more two-dimensional, as found by both experiment[10] and theory.[25]

Precise $E(k_x)$ band dispersions are obtained by fitting the peaks of individual momentum distribution curves (MDCs) and energy distribution curves (EDCs). These correspond to horizontal and vertical cuts through Fig. 2 top, respectively (samples of MDCs and EDCs are given in Figs. 4 and 5). For steep bands the MDCs are more accurate because they produce sharp peaks (open circles in Fig. 2 bottom). For flat bands, on the other hand, the EDCs exhibit sharp peaks and thus provide clearer information (open squares). The consistency between MDCs and EDCs is tested in the transition region between steep and flat sections of a band. For the lower band we add results from our previous work[10,12] for completeness (open triangles).

The fairly complex set of features can be reduced to three bands **1′**,**1″**,**2** by utilizing our highly-redundant data which cover several Brillouin zones (Fig. 2). The labels **1′**,**1″**,**2** are used by analogy to bands with comparable dispersion at stepped Si(111) surfaces.[22] Band **2** extends from −1.25 to −0.3 eV, band **1″** from −0.17 to −0.04 eV, and band **1′** from −0.6 eV to E_F, with a Fermi velocity $v_F=0.74\times10^6$ m/s and a Fermi wave vector $k_F=0.23$ Å^{-1} (slightly larger than the zone boundary A_4 at 0.205 Å^{-1}). These numbers are obtained by fitting analytic curves to the data points in Fig. 2 bottom. Bands **1′** and **2** are approximated by a tight binding model,[21,22] with band **2** truncated at its maximum of −0.3 eV. A cosine curve is used for band **1″**. The branch of band **1″** at negative k_x is used, because the branch at positive k_x is shifted down by 0.08 eV due to insufficient saturation of the photovoltage.

The most intense band by far is band **2**, which exhibits a 5×1 periodicity (full lines in Fig. 2). The actual 5×2 reconstruction would introduce backfolded replicas of band **2** (dashed lines in Fig. 2), which are too weak to be observed. That is consistent with the weak half-order streaks in the LEED pattern (Fig. 1). In contrast to stepped surfaces,[22] there is no evidence of a band splitting for band **2**. Furthermore, the Fermi level lies about 0.3 eV higher relative to band **2** for Si(111)5×2-Au than for the other Au chain structures, except Si(775)-Au. This significantly higher band filling is probably related to the fact that Si(111)5×2-Au and Si(775)-Au have two Au chains per unit cell, while the other chain structures have only one.[22]

The bands **1′** and **1″** both approach E_F near the 5×4 zone boundary A_4, although only band **1′** actually crosses the

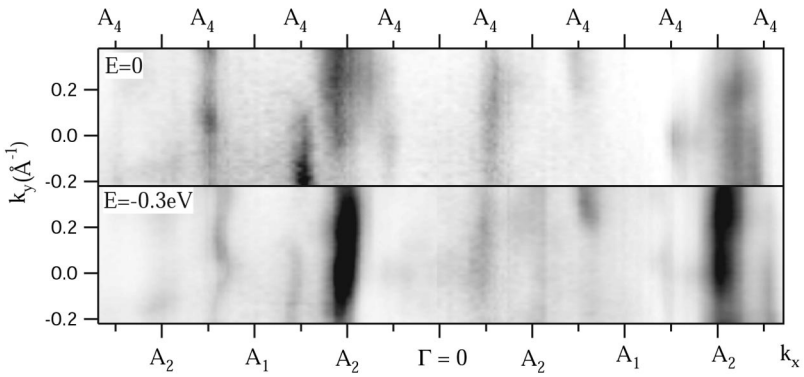

FIG. 3. Constant energy surfaces for Si(111)5×2-Au at the Fermi level and at the top of band **2**. The Fermi surface consists of straight, one-dimensional sections with strong intensity modulations along k_y. These are all located near the 5×4 zone boundaries A_4, as long as the background from the high energy tail of band **2** at the A_2 points is subtracted. Horizontal cuts through the energy surfaces are given in Fig. 4.

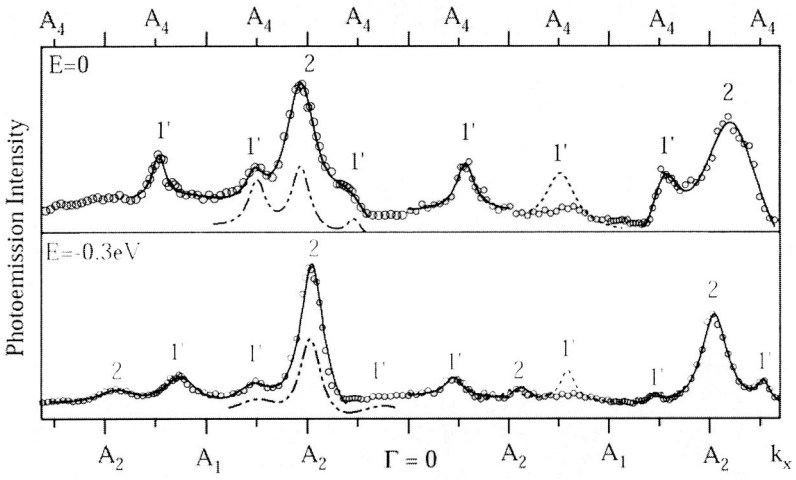

FIG. 4. MDCs across the constant energy surfaces in Fig. 3 at various k_y (full lines and circles at $k_y=0$, dashed lines at $k_y=+0.32$ Å^{-1}, dot-dashed lines at $k_y=-0.16$ Å^{-1}). The density of states near the Fermi level exhibits peaks near the 5×4 zone boundaries A_4. These are able to stabilize a 5×4 lattice via the opening of a small gap at E_F. Such a periodic 5×4 interaction has been found between extra Si atoms on top of the 5×2 chains.[29]

Fermi level within our photovoltage uncertainty of 0.08 eV. Band **1″** begins 0.04 eV below the top of band **1′**. Band **1′** is very similar to the metallic, $\frac{1}{4}$-filled band found on Si(553)-Au.[21,22] In both cases one observes a free-electron-like band dispersing straight through E_F. Band **1″**, on the other hand, curves back when approaching E_F. It can be extended to the other half of the 5×2 Brillouin zone by a cosine function with 5×4 periodicity. Band **1″** may be viewed as a continuation of band **2** beyond the point of half filling when using the 5×1 unit cell.

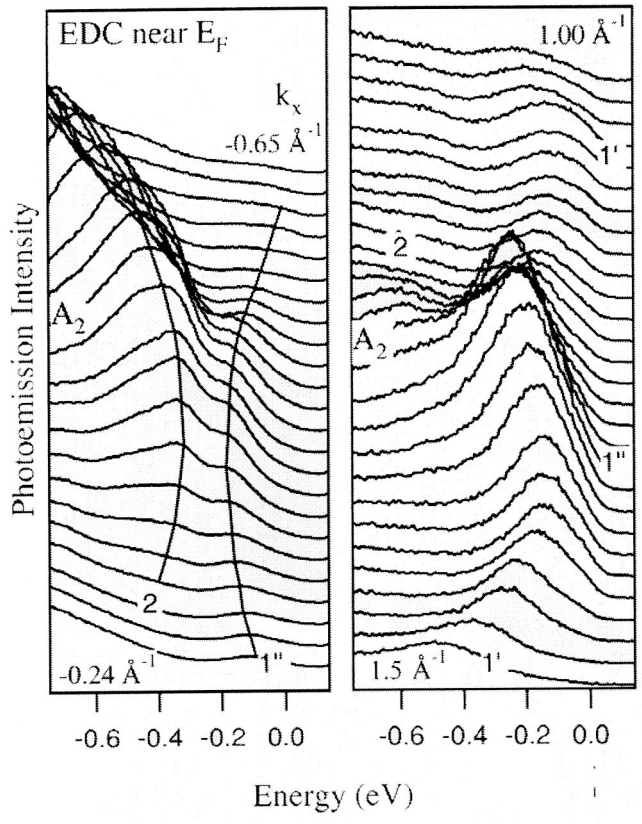

FIG. 5. EDCs for states near the 5×2 zone boundaries A_2, showing bands **1″** and **2** with a small gap of 0.13 eV in between (left). The EDCs are dominated by the flat bands (**1″**), while the MDCs in Fig. 4 are dominated by steep bands (**1′**). The gray scale image in Fig. 2 shows both.

As refinement we introduce the 5×2 Brillouin zone, which corresponds to the 5×2 reconstruction of the underlying chains. It is responsible for the mini-gap of 0.13 eV between band **2** and band **1″**, as well as the symmetry of band **1″** about the 5×2 zone boundary A_2. In the 5×2 model the interpretation of the bands is a bit different. Band **2** is now completely filled inside the smaller 5×2 zone, and its continuation above E_F—0.3 eV is now a separate band **1″**. The minigap of 0.13 eV between bands **2** and **1″** can be seen directly in the EDCs of Fig. 5 (left). The 5×2 interaction potential $V_{5\times2}$ is half of the minigap, i.e., $V_{5\times2}\approx0.065$ eV.

IV. THE 5×4 SUPERLATTICE BANDS NEAR E_F

The 5×4 lattice formed by the extra Si atoms on top of the chains doubles the unit cell once more. It is interesting to see that bands **1′** and **1″** both come closest to the Fermi level at the zone boundaries A_4 of the 5×4 unit cell (Figs. 2–4). Figure 3 shows that the bands form straight, one-dimensional lines. These are able to nest perfectly and thereby give rise to the strong instabilities that are characteristic of one-dimensional systems. In particular, they are able to trigger a 5×4 superlattice, such as that formed by the extra Si atoms on top of the chains.

For investigating the situation near the Fermi level more closely we plot constant energy surfaces in Fig. 3, i.e., the photoemission intensity versus k_x and k_y, where k_x runs along the chains and k_y perpendicular to them. The upper panel is taken at the Fermi level and the lower at −0.3 eV, the top of band **2**. The intensity of band **2** at the zone boundary A_2 is so high that its tail still contributes significantly to emission at the Fermi level. After discounting the intensity at the A_2 points in the upper panel of Fig. 3 we observe that all the other Fermi surface points lie along one-dimensional lines close to the 5×4 zone boundaries A_4. While there is a significant intensity modulation along k_y, the band does not disperse along that direction.

The Fermi level crossings are quantified in Fig. 4 (top panel), where MDCs along the chain direction k_x are plotted.

Because of the intensity variation with k_y we plot MDCs for three k_y values ($k_y=0$, $+0.32$, -0.16 Å^{-1}, with the Brillouin zone boundary at $k_y=\pm0.19$ Å^{-1}). Most of the peaks from bands **1′**, **1″** lie again close to A_4 points. Only two additional peaks are seen at A_2 points. They become much more pronounced when going down in energy from E_F to E_F—0.3 eV, where the top of the intense band **2** is located (bottom panel of Fig. 4). Therefore, they are assigned to the high energy tail of band **2** and not to a true Fermi surface feature.

V. DOPING OF THE CHAINS AND NANOSCALE PHASE SEPARATION

Recent local density calculations[25] have shown that the extra Si atoms provide extra electrons that dope the chains. The doping reduces the total energy of the structure, which reaches a minimum at a doping level of $\frac{1}{2}$ electron per 5×2 unit cell. According to the calculation, an extra Si atom is only able to use two of its four valence electrons for doping the chains. The other two valence electrons of Si are used up in backbonds, which correspond to bands many electronvolts below E_F. Thus, the optimum doping requires one Si adatom per 5×8 cell, and one would expect the formation of a 5×8 adatom lattice. Instead, the surface reconstructs into a half-filled 5×4 lattice fluid of Si adatoms.[29] The adatoms have a tendency to phase-separate into short 5×4 rows with empty 5×2 sections in between, each typically 5–10 nm long. Recent scanning tunneling spectroscopy (STS) work[16] shows that the empty 5×2 sections are metallic, and the 5×4 adatom sections semiconducting. The gap is about 0.6 eV but lies mostly above E_F. The 5×4 periodicity of the Fermi surface that we observe provides an elegant way to explain this tendency of nanoscale phase separation into 5×4 sections, instead of a homogeneous 5×8 lattice. Although favored by the electronic structure, the 5×4 sections filled with adatoms have twice the optimum doping and become unstable when too long. They get rid of their excess electrons by donating them to adjacent empty sections, which are underdoped. Such a charge transfer was suggested from the STS data.[16]

In view of these observations one should discuss the band structure observed in photoemission by two sets of bands, one for occupied, the other for empty sections. There are several ways to group the three observed bands into pairs. The most natural grouping assumes that bands **1′** and **2** form a pair. The third band (**1″**) either has a partner above E_F, or it is identical in both segments. This pairing fits well with our observation that bands **1′** and **2** have their minima both at the A_1 point, and their band dispersions (effective masses) are comparable (see Fig. 2). (The third band, on the other hand, has its minimum at A_2 and exhibits a significantly higher effective mass.) Since band **1′** is found to be metallic in photoemission it has to belong to the chain segments without extra Si atoms according to the STS data.[16] Consequently, band **2** represents the semiconducting sections with extra Si atoms. Band **2** lies deeper than its metallic partner **1′** and therefore has higher band filling. That is consistent with the prediction from total energy calculations that the extra Si atoms dope the surface with electrons.[25] The extra band filling in the doped segments is 1 electron per 5×2 Brillouin zone, with band **2** completely filled (2 electrons) and band **1′** half-filled (1 electron). Since the doped segments cover only half of the surface, the average doping becomes $\frac{1}{2}$ electron per 5×2 cell, exactly the optimum doping predicted by theory.[25]

The STS features can be identified to some degree with photoemission bands, although it is difficult to tell which part of k space is sampled in STS. Without going into details we note that the energy splitting between the metallic and semiconducting bands **1′** and **2** is about 0.7 eV, which is significantly larger than the splitting of about 0.2 eV between the features in STS. One would have to pair up A with C' in order to obtain a splitting comparable to that in photoemission. An additional question with this assignment is the role of band **1″**. For the correct doping this band would have to be common to both segments.

A second pairing of bands produces an absolute band splitting closer to that from STS, but gets into difficulties with explaining the order of the bands. In this case bands **1′** and **1″** are partners and the average splitting is only 0.2 eV (0.4 eV at the bottom, 0.0 eV at the top). The metallic band **1′** is again assigned to the empty, metallic chain segments. Its large Fermi velocity gives rise to a low, featureless density of states that could explain the background feature B' straddling the Fermi level in STS.[16] The semiconducting band **1″** matches feature B in the tunneling spectra, which corresponds to the semiconducting 5×4 adatom structure, including the close proximity of the valence band maximum to E_F. The fact that the minima of bands **1′** and **1″** occur at different k points (A_1 vs A_2) might be explainable by a strong surface umklapp of band **1″** due to the 5×4 superlattice (which connects A_1 and A_2). However, the semiconducting band **1″** now lies above the metallic band, which is opposite to the STS observation that the peaks in the semiconducting sections lie below their counterparts in the metallic sections. Band **2** is more difficult to assign with this pairing. Since there is no partner available for it, one must assume that it actually consists of an unresolved pair of bands, one for metallic and the other for semiconducting sections. That would associate the STS features A, A' both with band **2**. The correct doping could be explained by continuing the semiconducting band **1″** throughout the 5×2 Brillouin zone as cosine function with 5×4 periodicity, which would give it a filling of two electrons per 5×2 cell.

In summary, there are intriguing connections between the observed bands and the STS features, but a firm assignment requires additional confirmation, such as mapping the bands of the metastable, completely filled 5×4 structure.[28]

VI. RELATED PHOTOEMISSION RESULTS

Our results for the bands near E_F can be compared with previous photoemission data.[6,7,9,15] Already in the early work,[6,7] the strongest intensity near E_F was observed in the second Brillouin zone at $k_x\approx1.0$ Å^{-1}, which coincides with strong emission near E_F in our data. Comparing with the most recent Ref. 15, we can identify our band **2** with S_2 and

the combined bands **1′**, **1″** with S_1. However, we decompose S_1 into two bands, one metallic and the other semiconducting, while S_1 is interpreted as a single, semiconducting band in Ref. 15. The alternative between either semiconducting or metallic character stressed in Ref. 15 becomes a moot issue in view of the recent observation of a phase separation into metallic and semiconducting segments by scanning tunneling spectroscopy.[16] We feel that the steeply dispersing band **1′** is an excellent candidate for the metallic sections of the chains. This band is clearly visible in the gray scale plot of $E(k_x)$ in Fig. 2 (top) and in the MDCs of Fig. 4, but it tends to be overlooked in EDCs, where steep bands become blurred into broad peaks (Fig. 5). The results in Ref. 15 do not contain MDCs, and the $E(k_x)$ gray scale plots have a k resolution that is too coarse to fully resolve a steeply dispersing band.

Among the other Au chain structures on vicinal Si(111) there is one with a band structure particularly similar to that of Si(111)5×2-Au. This is Si(775)-Au, which is also based on two Au chains per unit cell, while the other structures have only one Au chain.[22] Both surfaces exhibit a strongly dispersing band that ends 0.3 eV below E_F, and a set of extra bands filling the region between band **2** and E_F. In the single chain structures, on the other hand, the analog to band **2** lies 0.3 eV higher and crosses E_F close to half filling. Some differences remain between Si(111)5×2-Au and Si(775)-Au, which reflect the extra row of broken bonds at the Si(775) step edge that changes the electron count. Band **2** is a doublet for Si(775) and a singlet for Si(111)5×2-Au. It exhibits strong backfolding at the A_2 zone boundary for Si(775) but none for Si(111)5×2-Au.

VII. SUMMARY

In summary, we have mapped out the band structure of Si(111)5×2-Au near the Fermi level in order to explore possible connections between one-dimensional Fermi surface instabilities and the surface reconstruction. The 5×4 lattice fluid of extra Si atoms is connected with a high density of one-dimensional states at the zone boundaries A_4 of the 5×4 lattice. Coupling between these nested Fermi lines creates a weak 5×4 lattice instability. Such a mechanism provides an intriguing explanation for the 5×4 inter-atomic potential of 1.2 meV that was derived from the correlation between extra Si atoms.[29] The observed minigap of about 400 meV is two orders of magnitude larger because only 1% of the electrons in the band experience an energy shift, i.e., those near the Fermi lines (for a two-dimensional analog, see Ref. 33). In order to pursue the connection between electronic structure and atomic potentials further it would be desirable to extend first principles calculations of Si—Au chain structures[24–26] to 5×4 and 5×8 superlattices.

Our observations have further implications when combined with first principles calculations predicting an optimum doping of 0.5 electron per 5×2 cell.[25] The mismatch between the adatom concentrations required for optimum doping and for a 5×4 superlattice explains the recently observed phase separation into metallic 5×2 chains without adatoms and semiconducting sections with a 5×4 superlattice of adatoms.[16] Without a 5×4 driving force from the Fermi surface one would expect a homogeneous 5×8 lattice of adatoms, instead of the observed 5×4 lattice covering only half of the surface. Our observation of two bands **1′** and **1″** near E_F fits into the two-phase model obtained by scanning tunneling spectroscopy.[16] Chain sections without adatoms can be assigned to the metallic band **1′** and sections with 5×4 adatom chains to the semiconducting band **1″**. However, an experiment with different lattice filling is required to rule out another possible assignment.

While a connection between electronic states and interatomic potentials has been made for many Peierls systems, there are two special aspects of the system considered here: (1) The interatomic potential is known experimentally, which allows quantitative comparisons. (2) The 5×4 periodicity of the Fermi surface competes with an ordered 5×8 superlattice required by the optimum doping and thereby gives rise to unusual phenomena, such as lattice fluid instead of an ordered superlattice and nanoscale phase separation. The electronic structure of such two-phase systems with nanometer phase separation will be an interesting avenue for the future. They have received attention in the context of stripe formation in two-dimensional systems of highly correlated electrons, such as high temperature superconductors. Gold-induced silicon chains represent an analog in one dimension.

ACKNOWLEDGMENTS

The authors acknowledge S. C. Erwin for insights on theoretical aspects, experimental help from A. Kirakosian, J.-L. Lin, and M. Fisher, and support from H. Weitering. The work was supported by the NSF under Award Nos. DMR-0240937 and DMR-0079983. It was conducted in part at the Synchrotron Radiation Center, which is supported by the NSF under Award No. DMR-0084402.

[1] G. Gruner, *Density Waves in Solids* (Perseus, Cambridge, MA, 1994), p. 259.
[2] J. Solyom, Adv. Phys. **28**, 201 (1979).
[3] T. Aruga, J. Phys.: Condens. Matter **14**, 8393 (2002).
[4] F.J. Himpsel, K.N. Altmann, R. Bennewitz, J.N. Crain, A. Kirakosian, J.L. Lin, and J.L. McChesney, J. Phys.: Condens. Matter **13**, 11097 (2001).
[5] E. Bauer, Surf. Sci. **250**, L379 (1991).
[6] I.R. Collins, J.T. Moran, P.T. Andrews, R. Cosso, J.D. Omahony, J.F. McGilp, and G. Margaritondo, Surf. Sci. **336**, 404 (1995).
[7] T. Okuda, H. Daimon, H. Shigeoka, S. Suga, T. Kinoshita, and A. Kakizaki, J. Electron Spectrosc. Relat. Phenom. **80**, 229 (1996).
[8] I.G. Hill, Phys. Rev. B **55**, 15 664 (1997).
[9] T. Okuda, H. Daimon, S. Suga, Y. Tezuka, and S. Ino, Appl. Surf. Sci. **121**, 89 (1997).
[10] R. Losio, K.N. Altmann, and F.J. Himpsel, Phys. Rev. Lett. **85**,

808 (2000).
[11] S. Hasegawa, J. Phys.: Condens. Matter **12**, R463 (2000).
[12] K.N. Altmann, J.N. Crain, A. Kirakosian, J.-L. Lin, D.Y. Petrovykh, F.J. Himpsel, and R. Losio, Phys. Rev. B **64**, 035406 (2001).
[13] F.J. Himpsel, K.N. Altmann, J.N. Crain, A. Kirakosian, J.L. Lin, and A. Liebsch, J. Electron Spectrosc. Relat. Phenom. **126**, 89 (2002).
[14] H.M. Zhang, T. Balasubramanian, and R.I.G. Uhrberg, Phys. Rev. B **65**, 165402 (2002).
[15] I. Matsuda, M. Hengsberger, F. Baumberger, T. Greber, H.W. Yeom, and J. Osterwalder, Phys. Rev. B **68**, 195319 (2003).
[16] H.S. Yoon, S.J. Park, J.E. Lee, C.N. Whang, and I.W. Lyo, Phys. Rev. Lett. **92**, 096801 (2004).
[17] P. Segovia, D. Purdie, M. Hengsberger, and Y. Baer, Nature (London) **402**, 504 (1999).
[18] R. Losio, K.N. Altmann, A. Kirakosian, J.-L. Lin, D.Y. Petrovykh, and F.J. Himpsel, Phys. Rev. Lett. **86**, 4632 (2001).
[19] I.K. Robinson, P.A. Bennett, and F.J. Himpsel, Phys. Rev. Lett. **88**, 096104 (2002).
[20] J.R. Ahn, H.W. Yeom, H.S. Yoon, and I.W. Lyo, Phys. Rev. Lett. **91**, 196403 (2003).
[21] J.N. Crain, A. Kirakosian, K.N. Altmann, C. Bromberger, S.C. Erwin, J.L. McChesney, J.L. Lin, and F.J. Himpsel, Phys. Rev. Lett. **90**, 176805 (2003).
[22] J.N. Crain, J.L. McChesney, F. Zheng, M.C. Gallagher, P.C. Snijders, M. Bissen, C. Gundelach, S.C. Erwin, and F.J. Himpsel, Phys. Rev. B **69**, 125401 (2004).
[23] D. Sanchez-Portal, J.D. Gale, A. Garcia, and R.M. Martin, Phys. Rev. B **65**, 081401 (2002).
[24] M.H. Kang and J.Y. Lee, Surf. Sci. **531**, 1 (2003).
[25] S.C. Erwin, Phys. Rev. Lett. **91**, 206101 (2003).
[26] D. Sanchez-Portal and R.M. Martin, Surf. Sci. **532**, 655 (2003).
[27] R. Bennewitz, J.N. Crain, A. Kirakosian, J.-L. Lin, J.L. McChesney, D.Y. Petrovykh, and F.J. Himpsel, Nanotechnology **13**, 499 (2002).
[28] A. Kirakosian, J.N. Crain, J.L. Lin, J.L. McChesney, D.Y. Petrovykh, F.J. Himpsel, and R. Bennewitz, Surf. Sci. **532**, 928 (2003).
[29] A. Kirakosian, R. Bennewitz, F.J. Himpsel, and L.W. Bruch, Phys. Rev. B **67**, 205412 (2003).
[30] J. Viernow, J.L. Lin, D.Y. Petrovykh, F.M. Leibsle, F.K. Men, and F.J. Himpsel, Appl. Phys. Lett. **72**, 948 (1998).
[31] J.N. Crain, K.N. Altmann, C. Bromberger, and F.J. Himpsel, Phys. Rev. B **66**, 205302 (2002).
[32] R. Losio, K.N. Altmann, and F.J. Himpsel, Phys. Rev. B **61**, 10 845 (2000).
[33] F. Schiller, J.C. Cordon, D. Vyalikh, A. Rubio, and J.E. Ortega (unpublished).